ACS APPLIED MATERIALS & INTERFACES

Research Article

www.acsami.org

Cicada-Wing-Inspired Self-Cleaning Antireflection Coatings on Polymer Substrates

Ying-Chu Chen, Zhe-Sheng Huang, and Hongta Yang*

Department of Chemical Engineering, National Chung Hsing University, 250 Kuo-Kuang Road, Taichung 40227, Taiwan

Supporting Information

ABSTRACT: The cicada has transparent wings with remarkable self-cleaning properties and high transmittance over the whole visible spectral range, which is derived from periodic conical structures covering the wing surface. Here we report a scalable self-assembly technique for fabricating multifunctional optical coatings that mimic cicada-wing structures. Spin-coated two-dimensional non-close-packed colloidal crystals are utilized as etching masks to pattern subwavelength-structured cone arrays directly on polymer substrates. The resulting gratings exhibit broadband antireflection performance and superhydrophobic properties after surface modification. The dependence of the cone shape and size on the antireflective and self-cleaning properties has also been investigated in this study.

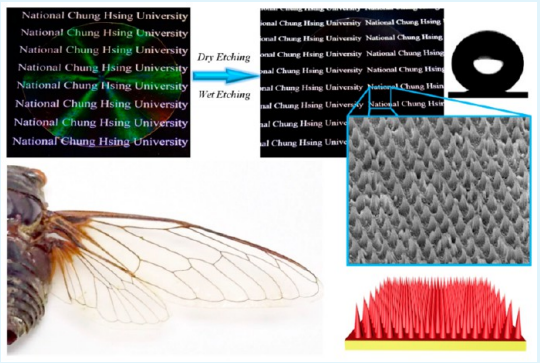

KEYWORDS: *cicada wing, self-assembly, colloidal crystal, antireflection, self-cleaning*

INTRODUCTION

In many optical products, traditional optical glasses have been replaced with polymer optics. The reasons that polymer materials are chosen include the low density, design freedom, configuration flexibility, and low cost of materials, which offer high manufacturability with satisfactory precision and fast repeatability.[1] Currently, optical-grade polymers are being thrust into the design forefront for sophisticated optical and electro-optical applications including goggles, hand-up displays, medical disposable optics, and bar-code scans.[2−4] Although most polymer materials have high visible transmittance, the Fresnel reflection occurs as light impinges at the air/polymer interface due to the discontinuity of the refractive index between air and polymers.[5] The light reflection from an optical surface can impair the legibility of displays, degrade performance of optical devices, and cause energy loss.[6] To address the issues, quarter-wavelength antireflection interference coatings and porous antireflection coatings (ARCs) are commonly used to eliminate the reflection.[7−9] However, the technologies suffer from complex fabrication processes, high cost, and limited material selection for different polymer substrates.[10]

Natural biological systems have developed many nanometer-scale architectures to produce striking optical effects by years of evolution.[11] For instance, cicada wings, which consist of hexagonal arrays of non-close-packed (NCP) sub-300 nm cones, are transparent and possess antireflective properties.[12] The conical structures with a period smaller than the propagating wavelength result in an effective refractive index gradient between air and the wings, suppressing the Fresnel reflection.[13,14] Similar to superhydrophobic lotus leaves, cicada wings are covered with a layer of epicuticular wax that restrains the penetration of water.[15−17] Furthermore, it is demonstrated that through the cooperation of NCP nanoscale cones preventing water drops from being trapped in the voids between wax-coated structures, the superhydrophobicity and self-cleaning functionality can be achieved on the wing surface.[18,19]

Inspired by the broadband antireflection performance of the low refractive index of cicada wings, numerous technologies have been extensively exploited for fabricating subwavelength-structured ARCs.[20] Nevertheless, current lithography-based fabrication technologies, including photolithography, nanoimprint lithography, and soft imprint lithography, in generating nanostructured ARCs are limited by the low resolution of small features and high cost of production.[21−23] In contrast, self-assembled blocked copolymers and colloidal crystals have been utilized as sacrificial masks to pattern periodic nanostructures, which renders a much simpler and inexpensive alternative in creating ARCs.[24] Unfortunately, most of the self-assembly methodologies, such as gravitational sedimentation, electrostatic repulsion, assembly at the liquid−air interface, evaporation-induced convective assembly, and template-assisted assembly, suffer from small areas, low throughput, and incompatibility with industrial-scale microfabrication.[25−31] In addition, only close-packed colloidal crystals are available through traditional self-assembly technologies, whereas NCP colloidal crystals are preferred for fabricating ARCs.[32]

Received: September 16, 2015
Accepted: October 27, 2015
Published: October 27, 2015

DOI: 10.1021/acsami.5b08743
ACS Appl. Mater. Interfaces 2015, 7, 25495−25505

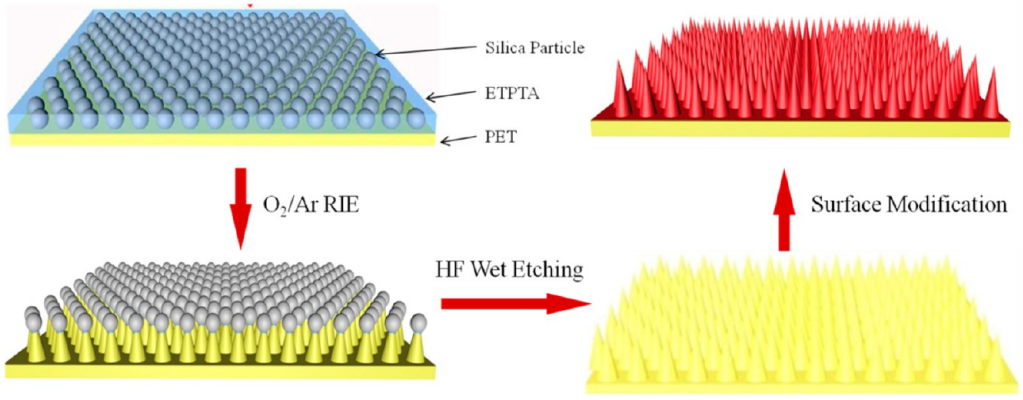

Figure 1. Schematic illustration of the experimental procedures for fabricating superhydrophobic cicada-wing antireflection coatings.

Recently, Jiang et al. developed a robust spin-coating technique that enables the production of NCP silica colloidal crystals on silicon wafers.[33] The silica particles serve as etching masks during a chlorine reactive ion etching (RIE) process to pattern silicon pillar arrays, which can then be used as second-generation templates to replicate subwavelength-structured polymer or glass ARCs.[34−36] However, the complex multistep fabrication process limits the mass production of practical ARCs on polymer subtracts.[35] Some problems in this soft-lithography-like replication remain to be solved, for example, deformation of the elastomeric stamp, density of defects in the formed pattern, and difficulty in high-resolution registration. Moreover, reproducible production of pillar arrays with high aspect ratio (ratio of the height to the width) for creating superhydrophobic ARCs is difficult to achieve.

To resolve the scale-up issue of current technologies, we demonstrate that the microfabrication-compatible spin-coating technology can be utilized for assembling monolayer NCP colloidal crystals on polymer substrates directly. The colloids can then be used to pattern polymer cone arrays for mimicking the nanostructures with micrometer-scale periodicity on the surface of cicada wings. The resulting gratings exhibit antireflection performance and large static water contact angles (SWCAs) through a surface modification procedure. Poly(ethylene terephthalate), commonly abbreviated PET, is one of the most common thermoplastic polymer resins and is used extensively for optical applications. Here, we systematically investigate the antireflective and superhydrophobic properties of templated cone arrays on PET substrates to ultimately implement transparent self-cleaning broadband ARCs on polymers.

EXPERIMENTAL SECTION

Materials and Substrates. The reagents used for the synthesis of silica microspheres include tetraethyl orthosilicate (TEOS) (98%), ammonium hydroxide (NH_4OH) (28%), ethanol (99.5%), and deionized water (18.2 MΩ cm). TEOS and NH_4OH were purchased from Sigma-Aldrich. Ethanol was obtained from Echo Chemicals. Deionized water was used directly from a Millipore A-10 water purification system. UV-curable ethoxylated trimethylolpropane triacrylate monomer (ETPTA, SR 454) and photoinitiator, Darocur 1173 (2-hydroxy-2-methyl-1-phenyl-1-propanone), were provided by Sartomer and BASF, respectively. (Tridecafluoro-1,1,2,2-tetrahydrooctyl)-trichlorosilane (97%) used for surface modification was purchased from Alfa Aesar. All chemicals and solvents were of reagent quality and were used without further purification. Poly(ethylene terephthalate) (PET) films (0.1 mm thick, Wisegate Technology) were used as coating substrates, which were rinsed with ethanol and then dried in a steam of nitrogen before use.

Synthesis of Silica Particles. Monodisperse silica microspheres with less than 5% diameter variation were synthesized according to the Stöber method.[37] In the present work, TEOS was hydrolyzed to form monodisperse silica particles in a mixture of ethanol, deionized water, and NH_4OH at room temperature over 1 day. The as-synthesized silica particles were purified in ethanol by multiple centrifugation/redispersion cycles to completely remove unreacted TEOS, deionized water, and NH_4OH.

Preparation of Silica Colloidal Suspensions. After centrifugation of a calculated volume of purified silica dispersion and discarding the supernatant solvent, silica microspheres were redispersed in nonvolatile ETPTA monomers (with 1 vol % photoinitiator) to make a final silica particle volume fraction of 20 vol % using a Thermolyne vortex mixer. After filtration through a 5 μm syringe filter (Whatman) to remove any particle aggregates, the transparent colloidal suspensions were collected in an open vial for 1 day to allow any residual ethanol to evaporate. Due to electrostatic repulsion between silica colloids in the ETPTA monomer (zeta potential of about −45 mV) and the refractive index matching between silica colloids and ETPTA monomer, which reduces the attractive van der Waals forces between colloids, the silica colloidal suspensions were stable for weeks.[38,39]

Fabrication of Monolayer Silica Colloidal Crystals by Spin Coating. One milliliter of silica colloidal suspension as prepared was dispensed on a PET substrate (10 cm × 10 cm), which was subjected to a rinse with ethanol before using. The PET film was tilted and rotated to spread the suspension to achieve full coverage and was then spin-coated at 1000 rpm for 20 s, 3000 rpm for 20 s, 6000 rpm for 20 s, and 8000 rpm for 180 s by using a spin-coater (WS-400B-6NPP-Lite spin process, Laurell). After spin-coating, the sample was transferred to a pulsed UV curing system (X Lite 500, OPAS) to photopolymerize ETPTA monomers by exposure to UV radiation for 10 s.

Templating Fabrication of Periodic Cone Arrays. The monolayer silica colloidal crystals were used as etching masks during a RIE process (40 mTorr chamber pressure, 20 sccm oxygen flow rate, and 20 sccm argon flow rate, and 100 W) to pattern arrays of cone-like structures directly on PET substrates. The templating silica particles finally could be removed by wet etching in a 1 vol % hydrofluoric acid aqueous solution for 1 min, followed by washing in ethanol.

Surface Modification of Periodic Cone Arrays. The hydrophobicity of the cone-covered polymer substrate could be further improved by surface functionalizing them with fluorosilane through chemical vapor deposition. The polymer substrate was placed in a sealed chamber, on the bottom of which was dispensed an unsealed beaker within a small amount of (tridecafluoro-1,1,2,2,-tetrahydrooctyl)-trichlorosilane. The chamber was then pumped to evaporate the fluorosilane to react with the hydroxyl groups on the surface of cone arrays.[40] After 1 h, the sample was moved to another clean sealed chamber and pumped to volatilize the unreacted fluorosilane molecules absorbed on the substrate.

DOI: 10.1021/acsami.5b08743
ACS Appl. Mater. Interfaces 2015, 7, 25495−25505

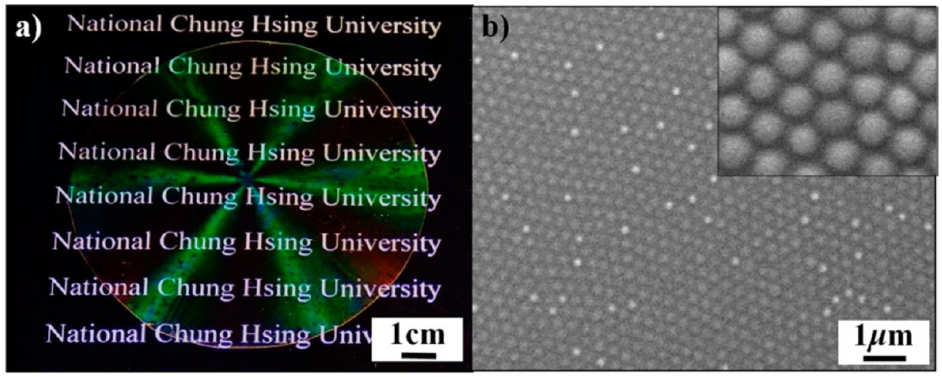

Figure 2. Nonclose-packed colloidal crystal on a PET substrate fabricated by the spin-coating technology. (a) Photograph of a specimen illuminated with white light. (b) Top-view SEM image. Inset shows a magnified SEM image.

Characterization. Field-emission scanning electron microscopy was carried out on a JEOL 6335F FEG-SEM. A thin layer of platinum was sputter-coated onto the specimens prior to imaging. A digital camera (Nikon Coolpix L810) was employed to acquire images of the specimens. Normal incidence optical reflection and transmission spectra were conducted using an Ocean Optics HR4000 high-resolution fiber-optic UV−visible−near-IR spectrometer. The spectra were recorded by Ocean Optics Spectra Suite Spectroscopy Software over a wavelength of 300−900 nm. Measurements were performed at normal incidence, and the cone angle of collection was less than 5°. The static water contact angles, advancing water contact angles, and receding water contact angles of the specimens were measured by a sessile drop shape analysis system (KRÜSS G10). Using an autopippetting system, 10 μL of deionized water was dispensed onto the specimen surface. The micropipette tip was then raised, and an image of the drop was taken. Analysis of each image yields a left and right contact angle. This process was repeated 9 times on different regions for each specimen, yielding 18 angle measurements per specimen. The average of these measurements was reported as the water contact angle.

RESULTS AND DISCUSSION

The schematic illustration of the templating procedures for preparing superhydrophobic polymer cone arrays is displayed in Figure 1. Two-dimensional silica colloidal crystal/ETPTA polymeric composites are assembled on PET substrates by a spin-coating technology, which is based on shear-aligning concentrated colloidal suspensions. This technological platform allows for scalable fabrication of hexagonally ordered colloidal monolayers with NCP structure and large domain size. The silica colloidal crystals function as etching masks during an oxygen−argon RIE process to pattern cone arrays directly on PET substrates. The nature of the mask is guided by the high selectivity of plasma etching between silica and polymer under/above RIE conditions.[41] The silica masks can then be selectively removed by wet-etching in a hydrofluoric acid aqueous solution. The aspect ratios and sizes of the as-fabricated polymer conical structures can be adjusted by controlling the RIE duration and the templating silica sphere diameter. The resulting cone arrays are finally functionalized to improve surface hydrophobicity by exposing to a vapor of (tridecafluoro-1,1,2,2-tetrahydrooctyl)-trichlorosilane with low surface energy. The silane coupling agent can be hydrolyzed with moisture to form reactive silanol groups and further condense with the hydroxyl groups on the surface of PET conical structures created by the RIE treatment.[42]

Figure 2a shows a photograph of a monolayer silica colloidal crystal−ETPTA composite consisting of 250 nm silica microspheres spin-coated on a PET substrate. Under white light illumination, it exhibits a characteristic six-arm pattern caused by Bragg diffraction of visible light from the hexagonal ordering and the NCP structure of the crystal, which is identical to that of spin-coated silica colloidal crystal on silicon wafers.[43] The crystal lattice structure is further confirmed by the top-view SEM image in Figure 2b. Although misaligned lines, which are mostly caused by silica spheres with distinct sizes, are observed, the long-range hexagonal arrangement of silica spheres is clearly evident from the SEM image. The periodic domain ordering can be achieved over centimeter-size area.

A brief oxygen/argon plasma etching process is then employed to etch the polymer matrix for 0.5, 1, 1.5, 2, and 2.5 min, respectively. Because the etching rate of silica is much lower than that of polymer, the periodically arranged silica spheres function as etching masks during the RIE process and protect the PET substrate immediately underneath them from being etched. As shown in Figure 3, we observe the NCP arrangement of mushroom-like features, consisting of top silica spherical caps and bottom PET conical stems. The cone-shape stems are caused by the isotropic etching of PET by reactive oxygen ions. Though longer RIE duration leads to the formation of sharper conical stems, the shrinkage of silica spheres is not significant. When the etching time reaches 2.5 min, the tops of the PET stems are too thin to support the above silica caps, resulting in damaged conical structures (Figure 3i). The templating silica caps can finally be selectively removed by wet-etching in hydrofluoric acid aqueous solution to create conical structure arrays directly on PET substrates. The cones at 2 min RIE duration have a height of ca. 560 nm and aspect ratio of ca. 2.2. By comparing Figures 2 and 3, it is evidenced that the long-range hexagonal ordering and the interparticle distance of the original spin-coated silica colloidal crystals are preserved throughout the templating procedure.

Theoretically, column-like structures exhibit narrowband antireflection since the refractive index does not transit smoothly at the air/substrate interface. This results in the optical properties of column-covered substrates being more related to that of traditional quarter-wavelength ARCs. In contrast, broadband antireflection performance can be achieved by changing the structural profile to create a gradual transition of refractive index from air to the bulk substrate. To evaluate optical properties of the templated PET cone arrays, an UV−visible−near-IR spectrometer is applied to measure the optical reflection and transmission at normal incidence. The lines in Figure 4a display the measured reflection from a bare PET film

DOI: 10.1021/acsami.5b08743
ACS Appl. Mater. Interfaces 2015, 7, 25495−25505

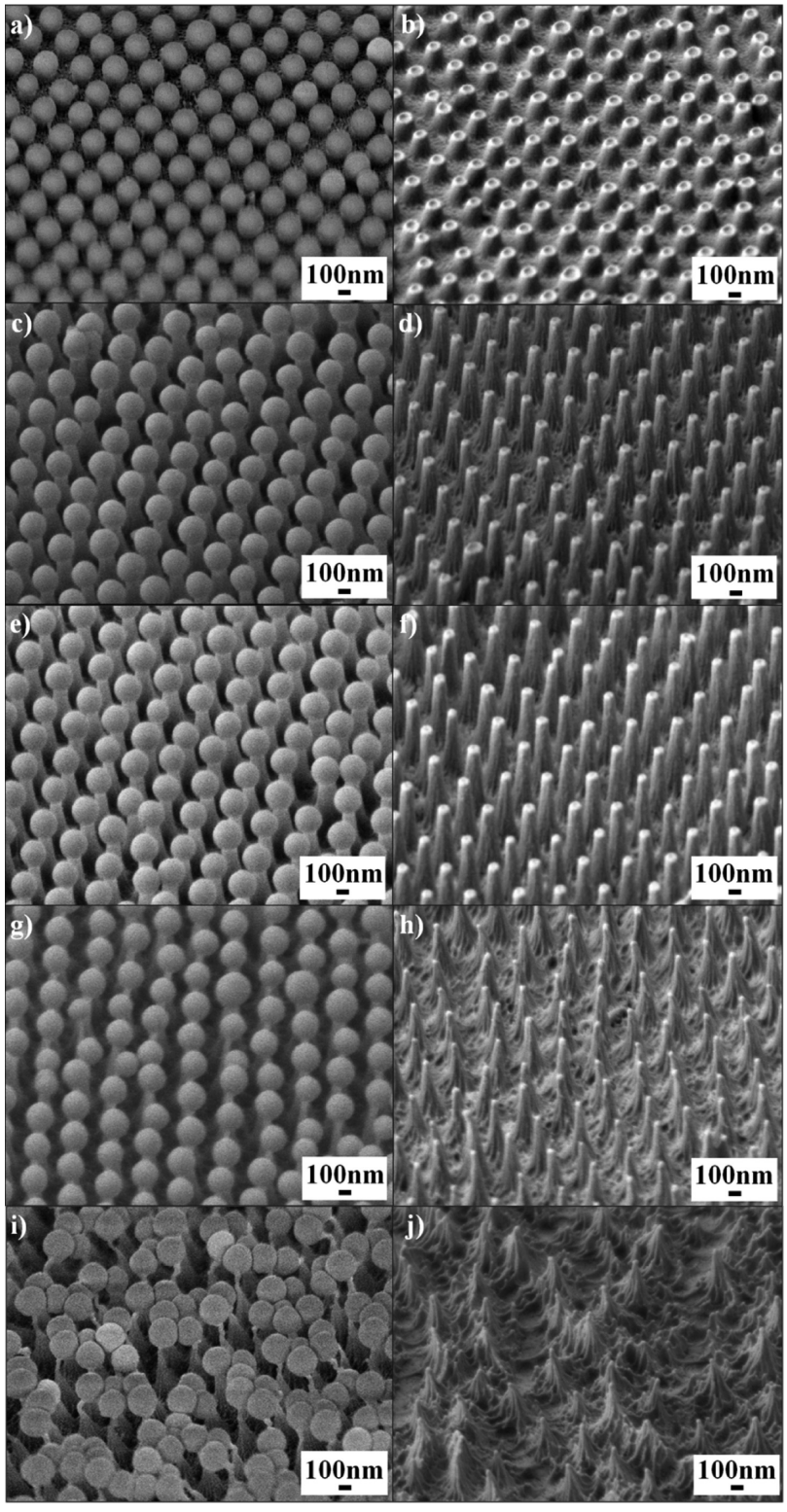

Figure 3. Tilted-view SEM images of mushroom-like structures and the corresponding PET conical structures templated from 250 nm silica spheres at different RIE durations. (a), (b) 0.5 min, (c), (d) 1 min, (e), (f) 1.5 min, (g), (h) 2 min, and (i), (j) 2.5 min.

and PET conical arrays templated from 250 nm silica spheres at different RIE durations as shown in Figure 3. As the reflection at normal incidence from an interface between two materials with refractive index of n_1 and n_2 is governed by Fresnel's equation ($R = (n_1 - n_2/n_1 + n_2)^2$), the featureless PET substrate exhibits a reflectivity of ca. 5% due to its refractive index of ca. 1.58. On the other hand, the reflection of PET cone-covered substrate after the 2 min RIE process reduces to less than 0.5% over the whole spectrum, indicating broadband antireflection.[7] It is also observed that longer RIE duration leads to lower reflection for all the above wavelengths, caused by a gradual transition of refractive index from air to the surface of sharp conical structures. Furthermore, the conical structures are damaged at 2.5 min RIE duration as shown in Figure 3j,

DOI: 10.1021/acsami.5b08743
ACS Appl. Mater. Interfaces 2015, 7, 25495−25505

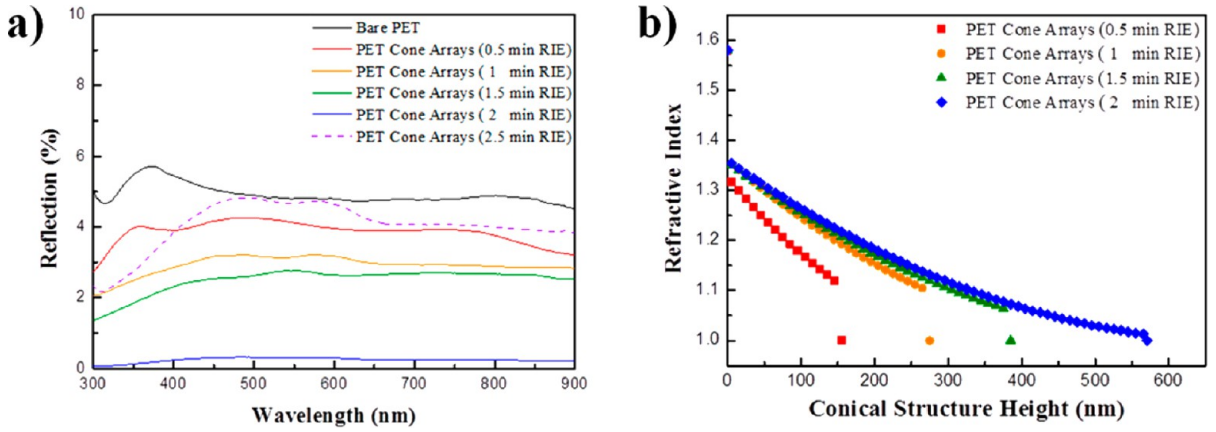

Figure 4. (a) Normal incidence optical reflection spectra obtained from a flat PET substrate and PET conical structures templated from 250 nm silica spheres at different RIE durations. (b) Comparison of the change of calculated effective refractive index from PET substrate (height = 0) to the top of the templated conical structure.

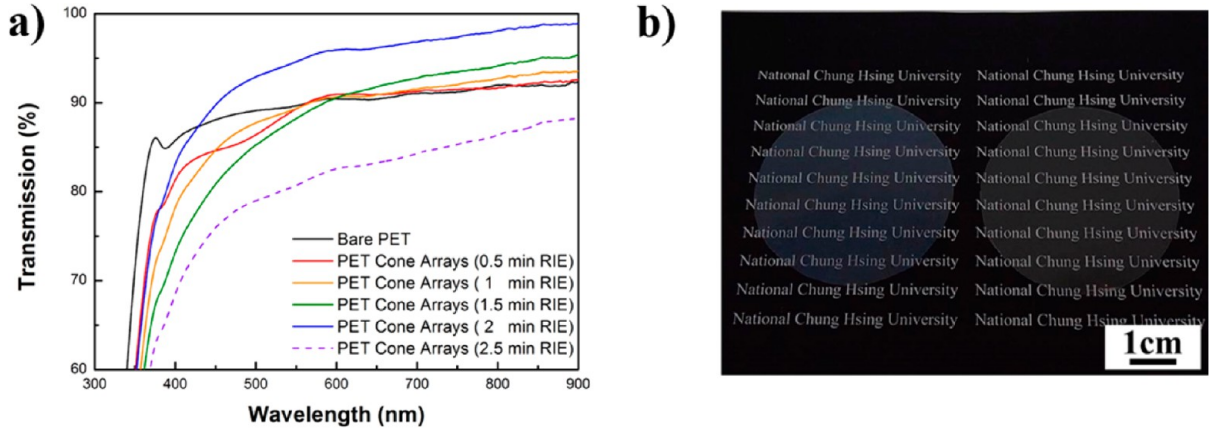

Figure 5. (a) Normal incidence optical transmission spectra obtained from a flat PET film and PET conical structures templated from 250 nm silica spheres at different RIE durations. (b) Photographic image of a flat PET substrate (left) and a PET cone-covered substrate after a 2 min RIE process (right).

resulting in the reflection of that (dashed line) greatly increasing to ca. 4.5%.

The cone lattice is hexagonal, and the distance between the centers of neighboring cones is $\sqrt{2}D$, where D is the diameter of templating silica spheres. Since the intercone distance is small with respect to the wavelength of light, light propagation is governed by the effective refractive index of the cone arrays. To understand the improved broadband antireflection performance for cone arrays, the calculated effective refractive index across the height of conical structures is mapped in Figure 4b. A cone-shaped profile that tapers smoothly from the base to vertex is used to simulate the templated structures as shown in Figure 3. The whole conical structure is divided into layers (10 nm layer thickness), and the refractive index of each layer can be evaluated from effective medium theory.[7] For the cones with less RIE durations, the effective refractive index decreases sharply. Meanwhile, for cones with 560 nm height (2 min RIE), the effective refractive index changes from 1.58 (PET substrate) to 1.36 (the base of cones) and then decreases more smoothly to 1 (air). The smooth refractive index gradient exhibited by the conical structures leads to very low reflection over a wide range of wavelengths.

Besides, the normal incidence transmission spectra of the samples are disclosed in Figure 5a. It is apparent that the transmission of PET cone-covered substrate increases with RIE duration, though the transmission of PET substrate at 2.5 min RIE duration (the dashed line) drops greatly due to light scattering caused by damaged conical structures. The PET substrate at 2 min RIE duration displays ca. 7% higher transmission in average over the whole visible spectrum than that of bare PET film. Moreover, a significant drop in transmission occurs in the wavelength range between 300 and 350 nm. The reason for this sudden decrease in transmission is caused by optical adsorption of the PET substrate in the corresponding wavelength range.[44] Figure 5b displays a photograph of a PET cone-covered substrate at 2 min RIE duration (right) and a flat PET substrate (left) illuminated with white light. The PET substrates here are cut to be circular to fit inside of the reactive ion etcher chamber which requires samples to have a maximum diameter of 4 in. Comparing with bare PET substrate exhibits milky color resulting from Fresnel's reflection, and the PET cone-covered substrate is less milky and macroscopically uniform for a few square centimeters, where the letters underneath the substrate are clearly visible through that. The transparent sample further confirms that incident visible light is not reflected from the PET cone-covered substrate. This suggests that large domain size transparent broadband ARCs can be fabricated by the spin-coating technology.

DOI: 10.1021/acsami.5b08743
ACS Appl. Mater. Interfaces 2015, 7, 25495−25505

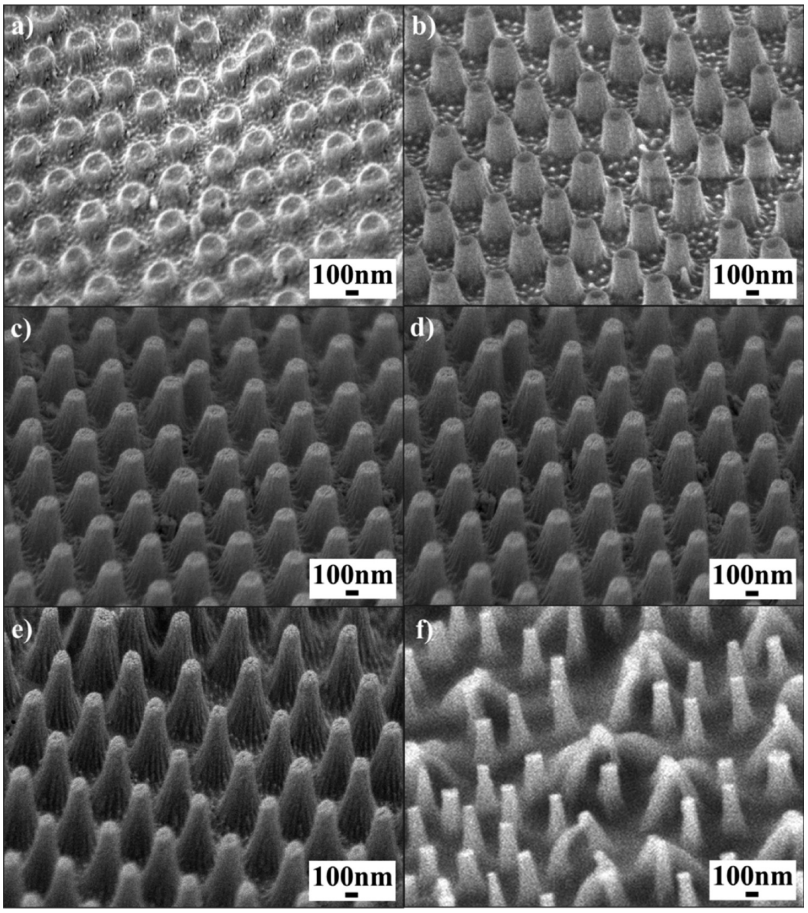

Figure 6. Tilted-view SEM images of the PET conical structures templated from 300 nm silica spheres at different RIE durations. (a) 0.5 min, (b) 1 min, (c) 1.5 min, (d) 2 min, (e) 2.5 min, and (f) 3 min.

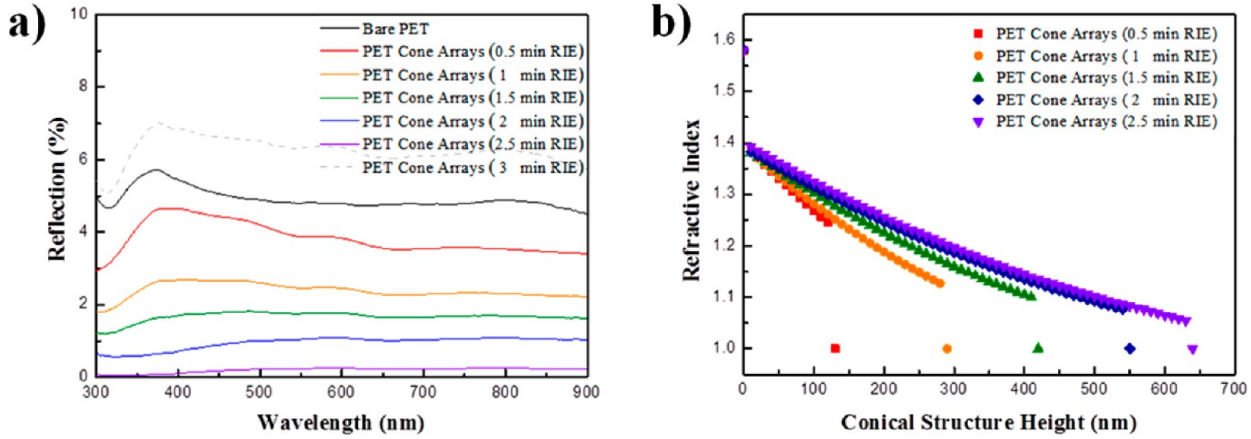

Figure 7. (a) Normal incidence optical reflection spectra obtained from a flat PET substrate and PET conical structures templated from 300 nm silica spheres at different RIE durations. (b) Comparison of the change of calculated effective refractive index from PET substrate (height = 0) to the top of the templated conical structure.

To gain a better understanding of the adjustable broadband antireflection properties, a monolayer NCP colloidal crystal consisting of 300 nm silica spheres or 200 nm silica spheres is introduced to pattern conical structure arrays, respectively. Figure 6 illustrates the hexagonally ordered cone arrays templated from 300 nm silica spheres at different RIE durations, followed by a wet-etching procedure. It is observed that the height of the conical structure increases with RIE duration, and the structures are collapsed as the dry-etching time reaches 3 min. The 0.5 min etched cones have vertical sidewalls, while the 2.5 min etched cones are tapered. As shown in Figure 6e, cones with height of ca. 640 nm and aspect ratio of ca. 2.1 can be achieved. Comparing the conical structures as shown in Figure 3 and Figure 6, it demonstrates that the templating silica sphere size does not affect the aspect ratio of as-prepared conical structures significantly, though higher conical structures can be achieved from larger templating silica spheres. That is reasonable as the width of the conical structure

DOI: 10.1021/acsami.5b08743
ACS Appl. Mater. Interfaces 2015, 7, 25495−25505

base templated from 300 nm silica spheres is larger than that templated from 250 nm silica spheres since the protected area underneath etching masks is proportional to the particle size during the RIE process.

Spectral reflectance measurements of the templated PET cone arrays at different RIE durations are carried out at normal incidence. Figure 7a illustrates the excellent control over the antireflection performance of the cone arrays by simply adjusting the RIE time. The height of the templated conical structure increases with etching time, leading to a gradual transition of refractive index at the interface between air and the PET substrate as displayed in Figure 7b. This results in the cone arrays (purple line in Figure 7a) displaying much lower reflectivity than that of a flat control sample (black line) for the whole visible spectrum. Besides, it is observed that the damaged conical structures at 3 min RIE duration cause the increase of reflection (dashed line).

Although the normal incidence transmission of PET cone-covered substrate increases with RIE duration (Figure 8), it is

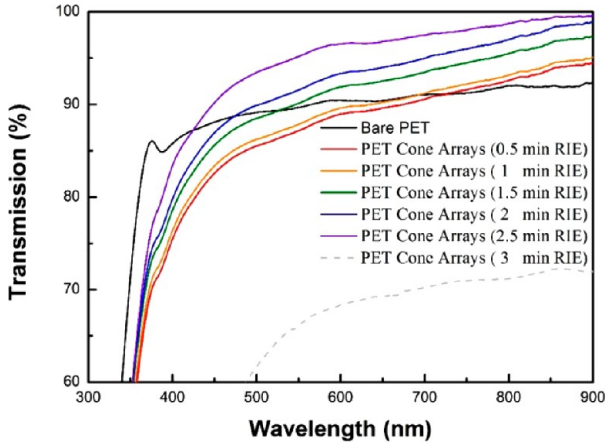

Figure 8. Normal incidence optical transmission spectra obtained from a flat PET film and PET conical structures templated from 300 nm silica spheres at different RIE durations.

validated that the resulting coatings show lower transmissions than that of a bare PET substrate. The reason is that the intercone distance and the size of the conical structures templated from 300 nm silica spheres have roughly the same scale as the wavelength of incident visible light. When light rays interacting wih periodic conical structures, part of the rays are reflected at the structure surface, and part of that is refracted. The refracted rays may be lost by absorption within the conical structures or emerge after several internal reflections. Hence, the incident light in the form of propagating energy is scattered off the cone arrays, indicating the coatings have lower transmissions.

To further enhance the transparency of the cicada-wing inspired ARCs, 200 nm silica spheres are introduced to pattern cone arrays. As shown in Figure 9, the conical structures with height of ca. 400 nm and aspect ratio of ca. 2 can be achieved at 1.5 min etching duration, while the formation of damaged conical structures can be found at 2 min etching duration. Besides, the size of the as-fabricated conical structures is smaller than those templated from 250 nm silica spheres and 300 nm silica spheres. Though some irregular tapered structures, caused by extra size of templating silica spheres, are observed, the hexagonal ordering of PET cones is clearly evident.

Figure 10a compares the spectral reflectances from a flat PET substrate and the templated PET cone arrays at different RIE durations. The normal-incidence reflection is greatly decreased from ca. 5% for a featureless PET substrate to less than 0.5% for the templated cone arrays at 1.5 min RIE duration. Once again, the gradual transition of refractive index at the air/PET interface (Figure 10b) results in the cone array coating exhibiting excellent broadband antireflection properties. Interestingly, it is apparent that the damaged conical structures at 2 min RIE duration do not affect the antireflection performance significantly. This is rational as the intercone distance and the cone size are small compared to the wavelength of visible light, so that light propagation is mainly governed by the effective refractive index of the cone arrays. Moreover, the optical properties obtained from the PET conical structures templated from 200 nm silica spheres at 2.5 min RIE duration are evaluated in Figure S1. The conical structures are seriously damaged at 2.5 min RIE duration as shown in Figure S1a, resulting in the normal incidence optical reflection greatly increasing to ca. 4% (Figure S1b). The results further demonstrate that the degree of damage of the templated conical structures also affects the antireflection performance.

Moreover, Figure 11a reveals that the transmission of the PET cone-covered substrate increases with RIE duration. Although the transition of refractive index of the as-prepared conical structure is not as smooth as those templated from larger silica spheres, a transmission larger than 97% in average over the visible light wavelength spectrum can be achieved. This agrees with the optical properties resulting from the nanostructures on the surface of the cicada wing.[12] The photographic image of the PET cone-covered substrate at 1.5 min RIE duration is displayed in Figure 11b. The highly transparent sample further demonstrates that incident visible light is not scattered off the as-prepared PET cone arrays. This suggests that large domain scale cicada-wing-inspired transparent broadband ARCs can be fabricated.

Since the templated cicada-wing ARCs are directly patterned on the polymer surface and no foreign materials need to be deposited on the substrates as in quarter-wavelength ARCs, an advantage of the resulting coatings is their high environmental stability. As observed in cicada wings, the wax-coated nanostructures can also lead to superhydrophobicity, which is a merit to reduce the dust contamination and to improve the flight capability. To further improve the stability of the as-fabricated ARCs under variable nature of the weather and environmental conditions, the resulting cone arrays are functionalized with fluorosilane through silane coupling reaction.

The SWCAs of the surface-modified conical structures templated from 300 nm silica spheres at different RIE durations as shown in Figure 12a are obtained by averaging 18 measurements on any individual sample. It is clear that the SWAC increases until a maximal contact angle of 156.9° (inset of Figure 12a) is achieved at a plasma etching time of 2.5 min, which significantly enhanced from ca. 72.5° on unfunctionalized bare PET substrates. For longer RIE duration, the formation of damaged nanostructures reduces the SWCA. The wettability on structured hydrophobic materials can be explained by using the Cassie model, which has been widely adopted for predicting the incomplete wetting on a composite consisting of both solid and trapped air.[45] In this study, the observations are qualitatively described by the Cassie equation

DOI: 10.1021/acsami.5b08743
ACS Appl. Mater. Interfaces 2015, 7, 25495−25505

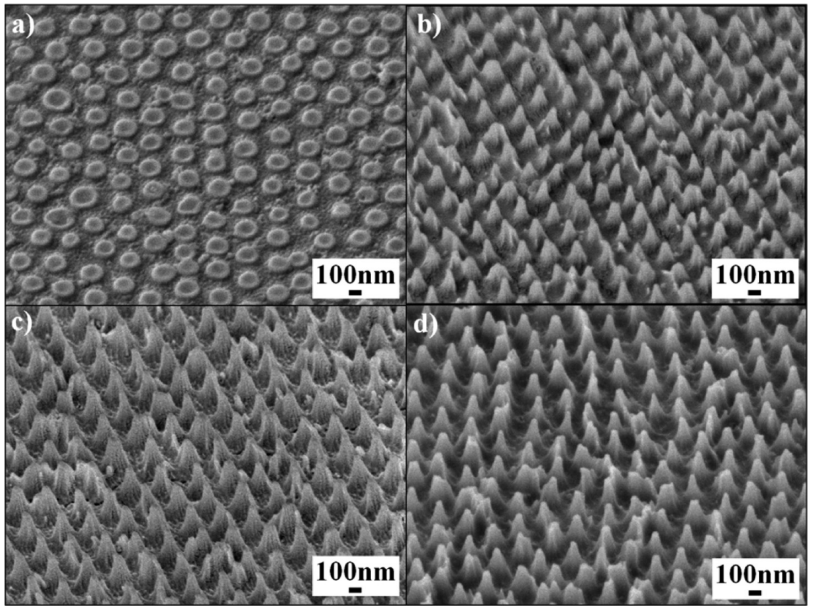

Figure 9. Tilted-view SEM images of the PET conical structures templated from 200 nm silica spheres at different RIE durations. (a) 0.5 min, (b) 1 min, (c) 1.5 min, and (d) 2 min.

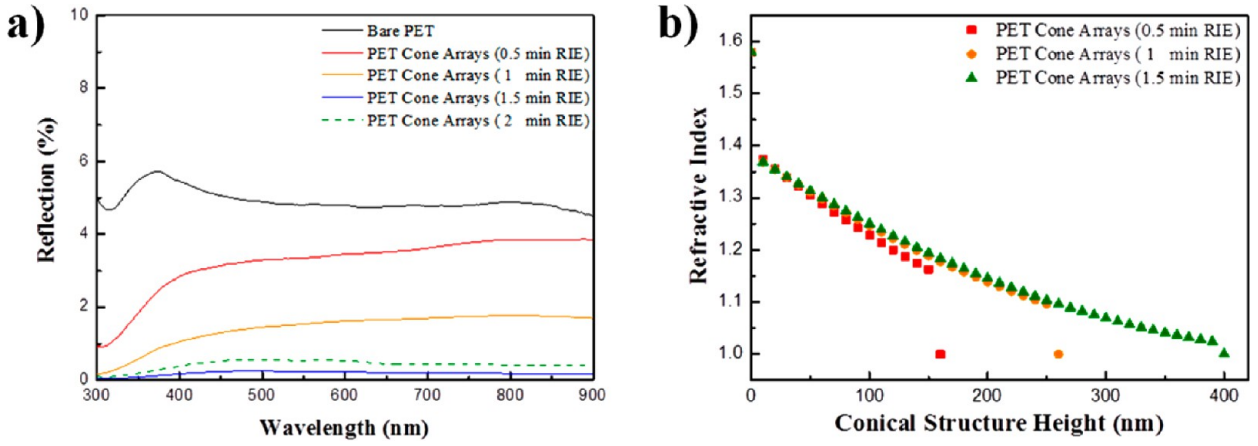

Figure 10. (a) Normal incidence optical reflection spectra obtained from a flat PET substrate and PET conical structures templated from 200 nm silica spheres at different RIE durations. (b) Comparison of the change of calculated effective refractive index from PET substrate (height = 0) to the top of the templated conical structure.

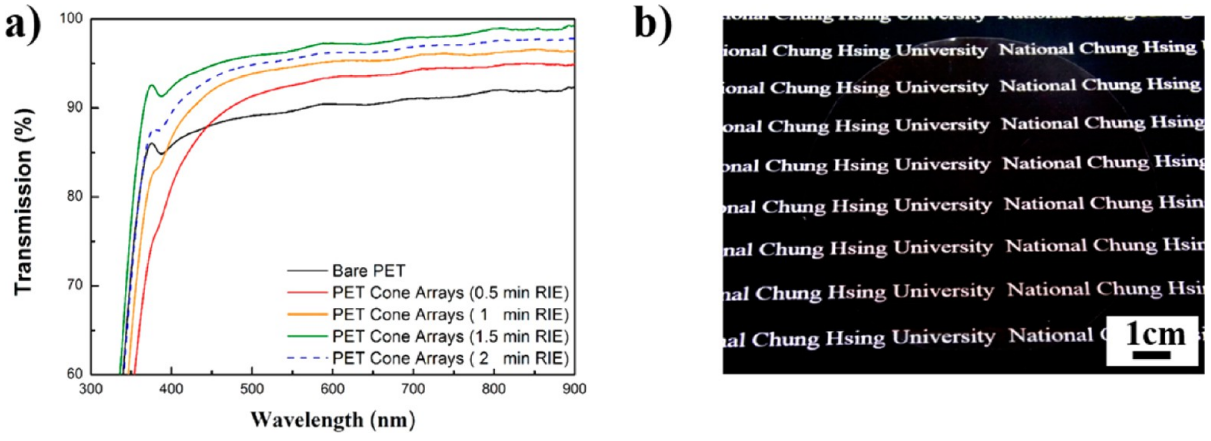

Figure 11. (a) Normal incidence optical transmission spectra obtained from a flat PET film and PET conical structures templated from 200 nm silica spheres at different RIE durations. (b) Photographic image of the PET cone-covered substrate after 1.5 min RIE process.

DOI: 10.1021/acsami.5b08743
ACS Appl. Mater. Interfaces 2015, 7, 25495−25505

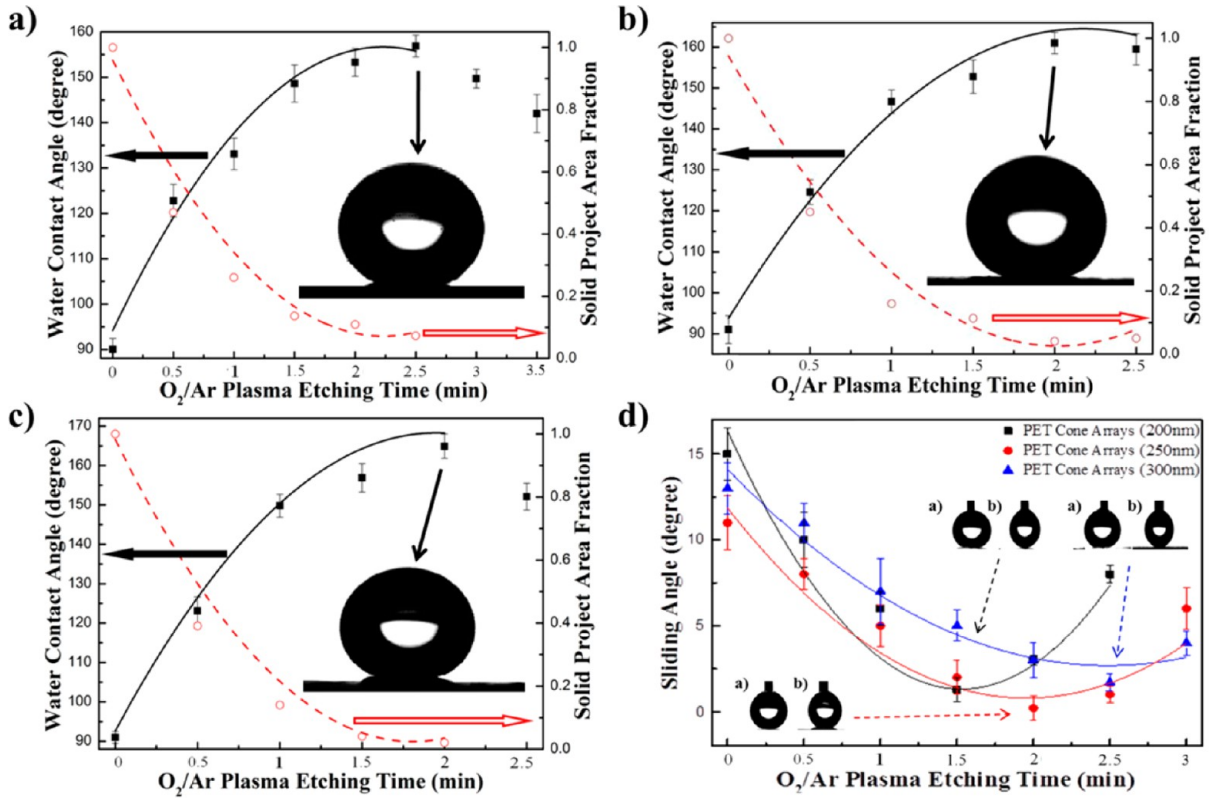

Figure 12. Dependence of the water contact angle and the projected area fraction of conical structures templated from (a) 300 nm, (b) 250 nm, and (c) 200 nm silica spheres at different RIE durations. (d) Sliding angles for the corresponding conical structures.

$$\cos\theta' = f\cos\theta - (1 - f) \quad (1)$$

where θ' is the SWAC on a rough surface; θ is the intrinsic WCA on a flat surface; and f is the fraction of the area of the polymer in direct contact with the water droplet out of the projected area. Figure 12a also displays estimated f at different RIE durations by using the following trigonometric calculation as

$$f = \frac{n\pi b^2}{\text{Unit Projected Area}} \quad (2)$$

where n is the number of cones on the unit projected area, and b is the radius of the top surface area of a conical structure measured by the SEM images shown in Figure 6. It is apparent that f value decreases with the increase of etching time and reaches a minimum value at a plasma etching time of 2.5 min. The calculated SWCAs using Cassie's equation are then compared with the experimental data in Figure 12a. The tendencies of calculated data (black solid line) and experimental results (black solid squares) are similar, indicating that a high fraction of air is trapped in the trough space between functionalized periodic conical structures, and the water droplet is therefore preventing it from contacting the substrates. Further experimental data and theoretical predictions, as shown in Figure 12b and Figure 12c, reveal that PET conical structures templated from 250 nm silica spheres and 200 nm silica spheres exhibit similar dewetting behaviors. That suggests the superhydrophobic ARCs with SWCA larger than 150° can be obtained, and the Cassie model is valid for the as-fabricated superhydrophobic surfaces.

Superhydrophobic surfaces are highly water repellent, and the nonwetting water tends to form spherical droplets that can roll off the surfaces with the application of a low tilting angle, carrying dirt away. To evaluate self-cleaning properties of the surface-modified PET cone-covered substrates, advancing contact angles and receding contact angles are measured by changing the volume of the water droplet on the substrate using the above sessile drop shape analysis system. The estimated sliding angles (difference between the advancing and receding contact angles) for the surface-modified PET cone-covered substrates etched at different RIE durations are then summarized in Figure 12d. It is observed that the sliding angle of the PET cone arrays templated from 300 nm silica spheres decreases with the increase of plasma etching time (blue line) and reaches a minimum value of 2° after 2.5 min RIE treatment. Once again, similar trends of the sliding angle with etching duration on surface-modified PET cone arrays templated from 250 nm silica spheres and 200 nm silica spheres are noticed. By comparing the results in Figure 12, it can be further validated that larger SWACs are associated with smaller sliding angles. This suggests that smaller water/substrate contact area results in smaller sliding angle. This study demonstrates that the superhydrophobic surface with a sliding angle less than 5° can be achieved on fluorosilane-modified PET cone-covered substrates.

Besides the self-cleaning functionality, the optical properties of the surface-modified PET cone-covered substrates are evaluated. The experimental reflection and transmission spectra obtained from the surface-modified PET conical structures templated from 200 nm silica spheres at 1.5 RIE durations in Figure S2 show similar transparency and reflectance performances to those of unmodified structures. The results disclose that the antireflection capability does not affect the surface

DOI: 10.1021/acsami.5b08743
ACS Appl. Mater. Interfaces 2015, 7, 25495−25505

modification process. This distinct combination is advantageous to develop self-cleaning ARCs.

SUMMARY

In conclusion, we have developed a scalable colloidal self-assembly technology for fabricating multifunctional subwavelength-structured optical coatings directly on polymer substrates that mimick the nanostructures of cicada wings. The templated cone arrays exhibit high transparency in the visible region and superior broadband antireflection, which can be determined by the size and shape of the templated conical structures. The cicada-wing-inspired antireflection coatings achieve superhydrophobic surface with high static water contact angle and small sliding angle after surface functionalization procedures, which are promising for creating self-cleaning transparent antireflection coatings on polymer substrates for a variety of technological applications in optical devices, solar cells, and protective coatings.

ASSOCIATED CONTENT

Supporting Information

The Supporting Information is available free of charge on the ACS Publications website at DOI: 10.1021/acsami.5b08743.

Figure S1: PET conical structures templated from 200 nm silica spheres at 2.5 min RIE duration. Figure S2: Surface modified PET conical structures templated from 200 nm silica spheres at 1.5 min RIE duration (PDF)

AUTHOR INFORMATION

Corresponding Author

*E-mail: hyang@dragon.nchu.edu.tw (H. Yang).

Notes

The authors declare no competing financial interest.

ACKNOWLEDGMENTS

Acknowledgment is made to Ministry of Science and Technology (Grant NSC 104-2221-E-005-086 and MOST 103-2622-E-005-017-CC3) for support of this research. The authors thank Professor Kun-Yi Lin from Department of Environmental Engineering, National Chung Hsing University, Taiwan, for his valuable discussion.

REFERENCES

(1) Hung, K. Y.; Liang, T. H. Application of Inclined-Exposure and Thick Film Process for High Aspect-Ratio Micro-Structures on Polymer Optic Devices. *Microsyst. Technol.* **2008**, *14*, 1217−1222.

(2) Koh, T. W.; Choi, J. M.; Lee, S.; Yoo, S. Optical Outcoupling Enhancement in Organic Light-Emitting Diodes: Highly Conductive Polymer as a Low-Index Layer on Microstructured ITO Electrodes. *Adv. Mater.* **2010**, *22*, 1849−1853.

(3) Doushkina, V.; Fleming, E. Optical and Mechanical Design Advantages using Polymer Optics. *Proc. SPIE* **2009**, *7424*, 74240Q1−74240Q12.

(4) Bormashenko, E.; Pogreb, R.; Stanevsky, O.; Biton, Y.; Bormashenko, Y. Self-Organization in Thin Polycarbonate Films and Its Optical and Electro-Optical Application. *J. Mater. Sci.* **2004**, *39*, 6639−6641.

(5) Biswas, K.; Gangopadhyay, S.; Kim, H.-C.; Miller, R. D. Nanoporous Organosilicate Films as Antireflection Coatings. *Thin Solid Films* **2006**, *514*, 350−354.

(6) Zhang, D.; Yu, W.; Hao, D.; Li, L.; Liu, H.; Lu, Z. Functional Nanostructured Surfaces in Hybrid Sol−Gel Glass in Large Area for Antireflective and Super-Hydrophobic Purposes. *J. Mater. Chem.* **2012**, *22*, 17328−17331.

(7) Macleod, H. A. *Thin-Film Optical Filters*; CRC Press: Boca Raton, FL, 2001.

(8) Boudot, M.; Gaud, V.; Louarn, M.; Selmane, M.; Grosso, D. Sol-Gel Based Hydrophobic Antireflective Coatings on Organic Substrates: A Detailed Investigation of Ammonia Vapor Treatment. *Chem. Mater.* **2014**, *26*, 1822−1833.

(9) Kitamura, S.; Kanno, Y.; Watanabe, M.; Takahashi, M.; Kuroda, K.; Miyata, H. Films with Tunable Graded Refractive Index Consisting of Spontaneously Formed Mesoporous Silica Nanopinnacles. *ACS Photonics* **2014**, *1*, 47−52.

(10) Schulz, U. Review of Modern Techniques to Generate Antireflective Properties on Thermoplastic Polymers. *Appl. Opt.* **2006**, *45*, 1608−1618.

(11) Srinivasarao, M. Nano-Optics in the Biological World: Beetles, Butterflies, Birds, and Moths. *Chem. Rev.* **1999**, *99*, 1935−1962.

(12) Sun, M.; Watson, G. S.; Zheng, Y.; Watson, J. A.; Liang, A. Wetting Properties on Nanostructured Surfaces of Cicada Wings. *J. Exp. Biol.* **2009**, *212*, 3148−3155.

(13) Lee, W.; Jin, M. K.; Yoo, W. C.; Lee, J. K. Nanostructured Metal Surfaces Fabricated by a Nonlithographic Template Method. *Langmuir* **2004**, *20*, 7665−7669.

(14) Xi, J. Q.; Schubert, M. F.; Kim, J. K.; Schubert, E. F.; Chen, M.; Lin, S. Y.; Liu, W.; Smart, J. A. Optical Thin-Film Materials with Low Refractive Index for Broadband Elimination of Fresnel Reflection. *Nat. Photonics* **2007**, *1*, 176−179.

(15) Bush, J. W.; Hu, D. L.; Prakash, M. The Integument of Water-Walking Arthropods: Form and Function. *Adv. Insect Physiol.* **2007**, *34*, 117−192.

(16) Hsu, S. H.; Woan, K.; Sigmund, W. Biologically Inspired Hairy Structures for Superhydrophobicity. *Mater. Sci. Eng., R* **2001**, *72*, 189−201.

(17) Bush, J. W. M.; Hu, D. L. Walking on Water: Biolocomotion at the Interface. *Annu. Rev. Fluid Mech.* **2006**, *38*, 339−369.

(18) Xu, Q. F.; Liu, Y.; Lin, F. J.; Mondal, B.; Lyons, A. M. Superhydrophobic TiO2−Polymer Nanocomposite Surface with UV-Induced Reversible Wettability and Self-Cleaning Properties. *ACS Appl. Mater. Interfaces* **2013**, *5*, 8915−8924.

(19) Milionis, A.; Giannuzzi, R.; Bayer, I. S.; Papadopoulou, E. L.; Ruffilli, R.; Manca, M.; Athanassiou, A. Self-Cleaning Organic/Inorganic Photo-Sensors. *ACS Appl. Mater. Interfaces* **2013**, *5*, 7139−7145.

(20) Raut, H. K.; Ganesh, V. A.; Nair, A. S.; Ramakrishna, S. Anti-Reflective Coatings: A Critical, In-Depth Review. *Energy Environ. Sci.* **2011**, *4*, 3779−3804.

(21) Heine, C.; Morf, R. H. Submicrometer Gratings for Solar Energy Applications. *Appl. Opt.* **1995**, *34*, 2476−2482.

(22) Chen, Q.; Hubbard, G.; Shields, P. A.; Liu, C.; Allsopp, D. W. E.; Wang, W. N.; Abbott, S. Broadband Moth-Eye Antireflection Coatings Fabricated by Low-Cost Nanoimprinting. *Appl. Phys. Lett.* **2009**, *94*, 263118.

(23) Groep, J.; Spinelli, P.; Polman, A. Single-Step Soft-Imprinted Large-Area Nanopatterned Antireflection Coatings. *Nano Lett.* **2015**, *15*, 4223−4228.

(24) Päivänranta, B.; Sahoo, P. K.; Tocce, E.; Auzelyte, V.; Ekinci, Y.; Solak, H. H.; Liu, C.-H.; Stuen, K. O.; Nealey, P. F.; David, C. Nanofabrication of Broad-Band Antireflective Surfaces Using Self-Assembly of Block Copolymers. *ACS Nano* **2011**, *5*, 1860−1864.

(25) Morhard, C.; Pacholski, C.; Lehr, D.; Brunner, R.; Helgert, M.; Sundermann, M.; Spatz, J. P. Tailored Antireflective Biomimetic Nanostructures for UV Applications. *Nanotechnology* **2010**, *21*, 425301.

(26) Yin, Y.; Lu, Y.; Gates, B.; Xia, Y. Template-Assisted Self-Assembly: A Practical Route to Complex Aggregates of Monodispersed Colloids with Well-Defined Sizes, Shapes, and Structures. *J. Am. Chem. Soc.* **2001**, *123*, 8718−8729.

DOI: 10.1021/acsami.5b08743
ACS Appl. Mater. Interfaces 2015, 7, 25495−25505

(27) Wong, S.; Kitaev, V.; Ozin, G. A. Colloidal Crystal Films: Advances in Universality and Perfection. *J. Am. Chem. Soc.* **2003**, *125*, 15589−15598.
(28) Denkov, N. D.; Velev, O. D.; Kralchevsky, P. A.; Ivanov, I. B.; Yoshimura, H.; Nagayama, K. Two-Dimensional Crystallization. *Nature* **1993**, *361*, 26−27.
(29) Dong, A.; Chen, J.; Vora, P. M.; Kikkawa, J. M.; Murray, C. B. Binary Nanocrystal Super Lattice Membranes Self-Assembled at the Liquid-Air Interface. *Nature* **2010**, *466*, 474−477.
(30) Lin, T. H.; Huang, W. H.; Jun, I. K.; Jiang, P. Bioinspired Assembly of Colloidal Nanoplatelets by Electric Field. *Chem. Mater.* **2009**, *21*, 2039−2044.
(31) Huang, Y.-F.; Jen, Y.-J.; Chen, L.-C.; Chen, K.-H.; Chattopadhyay, S. Design for Approaching Cicada-Wing Reflectance in Low-and High-Index Biomimetic Nanostructures. *ACS Nano* **2015**, *9*, 301−311.
(32) Stavenga, D. G.; Foletti, S.; Palasantzas, G.; Arikawa, K. Light on the Moth-Eye Corneal Nipple Array of Butterflies. *Proc. R. Soc. London, Ser. B* **2006**, *273*, 661−667.
(33) Jiang, P.; McFarland, M. J. Wafer-Scale Periodic Nanohole Arrays Templated from Two-Dimensional Nonclose-Packed Colloidal Crystals. *J. Am. Chem. Soc.* **2005**, *127*, 3710−3711.
(34) Sun, C. H.; Min, W. L.; Linn, N. C.; Jiang, B.; Jiang, P. Templated Fabrication of Large Area Subwavelength Antireflection Gratings on Silicon. *Appl. Phys. Lett.* **2007**, *91*, 231105.
(35) Min, W. L.; Jiang, B.; Jiang, P. Bioinspired Self-Cleaning Antireflection Coatings. *Adv. Mater.* **2008**, *20*, 3914−3918.
(36) Askar, K.; Phillips, B. M.; Fang, Y.; Choi, B.; Gozubenli, N.; Jiang, B.; Jiang, P. Self-Assembled Self-Cleaning Broadband Anti-reflection Coatings. *Colloids Surf., A* **2013**, *439*, 84−100.
(37) Stöber, W.; Fink, A.; Bohn, E. J. Controlled Growth of Monodisperse Silica Spheres in the Micron Size Range. *J. Colloid Interface Sci.* **1968**, *26*, 62−69.
(38) Min, W. L.; Jiang, P.; Jiang, B. Large-Scale Assembly of Colloidal Nanoparticles and Fabrication of Periodic Subwavelength Structures. *Nanotechnology* **2008**, *19*, 475604.
(39) Russel, W. B.; Saville, D. A.; Schowalter, W. R. *Colloidal Dispersions*; Cambridge University Press: U.K., 1989.
(40) Yang, H.; Jiang, P. Self-Cleaning Diffractive Macroporous Films by Doctor Blade Coating. *Langmuir* **2010**, *26*, 12598−12604.
(41) Junkar, I.; Modic, M.; Mozeti, M. Modification of PET Surface Properties using Extremely Non-Equilibrium Oxygen Plasma. *Open Chem.* **2015**, *13*, 490−496.
(42) Plueddemann, E. P. *Silane Coupling Agents*, 2nd ed.; Plenum Press: New York, 1991.
(43) Jiang, P.; McFarland, M. J. Large-Scale Fabrication of Wafer-Size Colloidal Crystals, Macroporous Polymers and Nanocomposites by Spin-Coating. *J. Am. Chem. Soc.* **2004**, *126*, 13778−13786.
(44) Wei, Y.; Ke, L.; Kong, J.; Liu, H.; Jiao, Z.; Lu, X.; Du, H.; Sun, X. W. Enhanced Photoelectrochemical Water-Splitting Effect with a Bent ZnO Nanorod Photoanode Decorated with Ag Nanoparticles. *Nanotechnology* **2012**, *23*, 235401.
(45) Cassie, A. B. D.; Baxter, S. Wettability of Porous Surfaces. *Trans. Faraday Soc.* **1944**, *40*, 546−551.

DOI: 10.1021/acsami.5b08743
ACS Appl. Mater. Interfaces 2015, 7, 25495−25505